Fifth International Conference on CFD in the Process Industries
CSIRO, Melbourne, Australia
13-15 December 2006

WAVE-STRUCTURE INTERACTION USING SMOOTHED PARTICLE HYDRODYNAMICS

Todd B. SILVESTER[1] and Paul W. CLEARY[1]

[1] CSIRO Mathematical and Information Sciences, Clayton, Victoria 3169, AUSTRALIA

ABSTRACT

Navier-Stokes computations of a wave-structure interaction are performed with the aim of assessing the potential of Smoothed Particle Hydrodynamics to accurately estimate impact loading time-history. A three-dimensional dam-break flow with a rectangular column located downstream is considered. The net force exerted on the column is monitored throughout the simulation with the results correlating well with existing experimental data. Simulation parameters including: particle resolution, fluid viscosity, gate opening times and boundary treatments are varied and their affect on the load imparted to the column are investigated.

NOMENCLATURE

$_{b,\,k}$	all 'fluid' and 'boundary' particles within a radius $2h$ of $\mathbf{r}$ respectively
c_s	sound speed
$\frac{D}{Dt}$	substantial derivative
$\boldsymbol{f}$	force per unit mass vector
$\boldsymbol{g}$	gravitational acceleration vector
h	interpolation length
I	Impulse of the net force
m_b, $\boldsymbol{r}_b$, $\boldsymbol{v}_b$	mass, position and velocity of particle b
n	number of particles
$\hat{\mathbf{n}}_k$	unit normal directed away from the boundary particle
P	dynamic pressure
$\lvert\mathbf{r}_\perp\rvert$ and $\lvert\mathbf{x}\rvert$	are the perpendicular and tangential distances from the boundary particle to the fluid particle
t	time
W	interpolation kernel
∇	differential operator
Δp	initial particle spacing
δt	simulation incremental time step
Π	viscous term
μ	dynamic viscosity
ρ	density

INTRODUCTION

The interaction of large waves with structures (slamming) is of importance to the maritime, naval and offshore industries (Faltinsen et al 2004). In large seas and heavy storms, waves can exceed the freeboard height and inflict serious damage to the superstructure and sensitive equipment on offshore installations and production ships (Ersdal & Kvitrud 2000). In the case of moored Floating Production Storage and Offloading Units (FPSO's) the wave-induced ship motions can cause further 'deck wetness' (or shipping of water) due to the relative motion between the vessel and waves. The presence of 'water on deck' is highly undesirable from a safety and operability standpoint and can result in loss of production and significant cost due to repairs and downtime.

Slamming phenomena are typically examined numerically though a series of simplified problems that possess certain features which resemble the fundamental flow behaviour. One such example is the dam-break problem. The dam-break approach consists of a volume of stationary water initially restrained by a gate. Upon releasing the gate, the body of water is free to flow under the influence of gravity. In such cases, the free-surface flow can resemble that of flow on a deck of a ship (Buchner 2002, Kleefsman et al 2005). Furthermore, the dam-break problem provides a useful test case for benchmarking free-surface numerical algorithms.

This paper presents Smoothed Particle Hydrodynamics (SPH) results of a free-surface dam-break flow and compares the calculated load on a square column located downstream to those measured during an experiment by Yeh and Petroff (see Gómez-Gesteira 2006). In recent times this configuration has proved to be a popular test case for benchmarking codes. This problem has appeared as a validation case for the recent SPH European Research Interest Group workshop (SPHERIC 2006). Previous comparisons have also been made using an Eulerian-Lagrangian Marker and Micro Cell (ELMMC-3D) method (Raad and Bidoae 2005) and SPH (Gómez-Gesteira and Dalrymple 2004).

THE SPH METHOD

SPH is a Lagrangian particle method that evaluates spatial derivatives of flow properties, (such as density and velocity) without the requirement of a computational grid. SPH discretises and represents the fluid (and or solid) as a series of pseudo-particles with the properties of the fluid (or solid) stored locally at the centre of each particle. Each particle represents an interacting mass point and also serve as interpolation points whereby the physical properties are calculated based on the information from neighbouring particles. Continuum properties at a particular point are interpolated (or smoothed) via a weighted sum of the properties of neighbouring particles; known as kernel interpolation. In other words, the interpolation kernel is applied to smooth (numerical distribute) the discrete values (e.g. density, pressure) at each particle over a finite region to provide a smooth and continuous interpolated field (e.g. density or pressure fields). The intrinsic advantages of SPH over conventional grid-based methods are that it can model very complex free-surface flows with impacts and structure interactions in a natural way. While SPH has it origins in astrophysical systems, (Gingold &

Monaghan 1977, Lucy 1977) in the last decade it has reached a high level of maturity in many complex industrial applications (Cleary et al 2005). The method is described in detail by Monaghan (1992, 1994, 2005) and only an overview of the essential features is presented here.

In discrete SPH form, the integral representation of a field function is approximated via the summation interpolant, given by,

$$A(\mathbf{r}) = \sum_{b=1}^{n} m_b \frac{A_b}{\rho_b} W\left(|\mathbf{r} - \mathbf{r}_b|, h\right) \tag{1}$$

where A is the interpolated function at position $\boldsymbol{r}$, the summation is over all (neighbouring) particles within $2h$ of $\boldsymbol{r}$ and W is the smoothing (or interpolating) kernel, in this case a cubic spline with radius $2h$ (Monaghan & Lattanzio 1985). From this definition, it follows that the gradient of function A can be written as,

$$\nabla A(\mathbf{r}) = \sum_{b=1}^{n} m_b \frac{A_b}{\rho_b} \nabla W\left(|\mathbf{r} - \mathbf{r}_b|, h\right) \tag{2}$$

Since W is an analytical function with continuous derivatives, the gradient of function A (Eqn. 2) can be calculated exactly without the requirement for a computational grid.

Continuity Equation

The SPH formulation used for this paper assumes the fluid is weakly compressible. That is, the fluid's sound speed is chosen to be 10 times greater than the maximum flow velocity. This ensures the density variations are small, less than 1%, and permits larger integration time steps. The form of the continuity equation used in the simulations is given by the time rate of change of density at a particle *'a'*,

$$\frac{D\rho_a}{Dt} = \sum_b m_b \mathbf{v}_{ab} \cdot \nabla_a W_{ab} \tag{3}$$

where $\mathbf{v}_{ab}$ denotes $\mathbf{v}_a - \mathbf{v}_b$, the gradient with respect to coordinates of particle a is ∇_a and the interpolation kernel is written as,

$$W_{ab} = W\left(|\mathbf{r}_a - \mathbf{r}_b|, h\right) \tag{4}$$

This form of the continuity equation is Galilean invariant and avoids anomalies at the free-surface associated with other forms of the continuity equation (Monaghan 1994).

Momentum Equation

The momentum equation (Navier-Stokes equation) for particle a expressed in vector notation is given by,

$$\begin{aligned} \frac{D\mathbf{v}_a}{Dt} = &-\sum_b m_b \left(\frac{P_a}{\rho_a^2} + \frac{P_b}{\rho_b^2} + \Pi_{ab} \right) \nabla_a W_{ab} \\ &- \sum_k m_k \Pi_{ab} \nabla_a W_{ak} + \sum_k \mathbf{f}_{ak} + \mathbf{g} \end{aligned} \tag{5}$$

where the summations are over *liquid-liquid* particle interactions and *liquid-boundary* particle interactions. The first term on the right hand side of Equation 5 represents the pressure and viscous acceleration interactions between fluid particles, the second term represents the viscous force per unit mass acting between the boundary particles and the fluid particle a. The third term represents the normal component of the boundary acceleration acting on the fluid particle to stop it penetrating the boundaries. The final term represents the gravitational acceleration component. The viscous formulation is given by (Cleary 1998),

$$\Pi_{ab} = \frac{\xi}{\rho_a \rho_b} \frac{4\mu_a \mu_b}{(\mu_a + \mu_b)} \frac{\mathbf{v}_{ab} \cdot \mathbf{r}_{ab}}{\mathbf{r}_{ab}^2 + \eta^2} \tag{6}$$

where ξ is a calibrated constant (Cleary 1998), $\mathbf{r}_{ab}$ denotes $\mathbf{r}_a$ - $\mathbf{r}_b$ and η is a small parameter used to remove the singularity at $\mathbf{r}_{ab}$ = 0. Similarly, for the viscous contribution between boundary particles '*k*' and adjacent fluid particles, Equation (6) is written with the dummy label *b* replaced with *k*.

Equation of State

The pressure is related to the variation in density via an equation of state. For the present simulations the equation of state is,

$$P = P_0 \left[\left(\frac{\rho}{\rho_0} \right)^{\gamma} - 1 \right] \tag{7}$$

where $\gamma = 7$, ρ_o is a reference density and P_0 is chosen so that the speed of sound is large enough to ensure the relative density fluctuations are small (< 0.01).

Physical Boundaries

The calculations are made using two separate treatments for the physical wall boundaries. In the first instance, the boundaries are defined by a single line of stationary particles that exert a normal repulsive force on fluid particles (Monaghan 1995). Throughout this paper, this boundary is referred to as "repulsive" and the boundary normal force acting on a fluid particle takes the form,

$$\mathbf{F}_{ak} = \frac{0.01 c_s^2 m_a}{h_{ak}} B(x) S(y) \hat{\mathbf{n}}_k \tag{8}$$

and the boundary potential term is written as,

$$S(y) = \begin{cases} \left[\left(\dfrac{sb}{s+2} \right) \dfrac{1}{q} \right]^s & \text{if } 0 \le q < \left(\dfrac{sb}{s+2} \right) \\ \left(\dfrac{s+2}{2b} \right)^2 (q-b)^2 & \text{if } \left(\dfrac{sb}{s+2} \right) \le q < b \\ 0 & \text{otherwise} \end{cases} \tag{9}$$

where $q = |\mathbf{r}_\perp| / h_{ak}$, $s = 8$ and b determines how far away from the wall boundaries the wall force is felt (i.e. "thickness" of the wall force); typically $b = 1$. The function $B(x)$ smoothes the force tangentially to ensure the fluid particle experiences a constant force as it travel parallel to the boundary particles.

$$B(x) = \begin{cases} 1 - \dfrac{|\mathbf{x}|}{\Delta p} & \text{for } 1 \le |x| \le \Delta p \\ 0 & \text{for } |x| > \Delta p \end{cases} \tag{10}$$

The second approach constructs the wall boundaries from two or more layers (depending on the kernel) of stationary fluid particles. These particles are included in the summations for the continuity equation and pressure terms of the momentum equations and their densities are

evolved. Throughout this paper, this boundary is referred to as “press./cont.”.

Time Stepping

The equations of motion (Eqns. 3 and 5) are a set of coupled ordinary differential equations and are integrated in time using a predictor-corrector scheme. The corrector step utilises a standard Euler scheme to project a full step using the previous step’s end-point rates of change. This can be summarised as follows, where **f** and D denote the time rates of change in velocity and density, respectively.

$$\begin{aligned} \mathbf{v}^{*} &= \mathbf{v}^{0} + \delta t\, \mathbf{f}^{0} \\ \mathbf{r}^{*} &= \mathbf{r}^{0} + \delta t\, \mathbf{v}^{0} \\ \rho^{*} &= \rho^{0} + \delta t\, D^{0} \end{aligned} \qquad (11)$$

Superscripts 0 and 1 denote the previous and current time step end-point values respectively. The time rates of change in the density and velocity are then calculated via Equations *3* and *5*. These end-point values are then used in the corrector to calculate the end point field values via a Backward Euler scheme.

$$\begin{aligned} \mathbf{v}^{1} &= \mathbf{v}^{0} + \delta t\, \mathbf{f}^{1} \\ \mathbf{r}^{1} &= \mathbf{r}^{0} + \delta t\, \mathbf{v}^{1} \\ \rho^{1} &= \rho^{0} + \delta t\, D^{1} \end{aligned} \qquad (12)$$

The size of the time step is chosen so that it satisfies the Courant condition modified for the presence of viscosity (Cleary 1998).

GEOMETRY AND SIMULATION DETAILS

The experiments performed by Yeh and Petroff (see Gómez-Gesteira 2006) utilized a rectangular tank 0.61 m wide, 1.6 m long and 0.75 m high with a 0.12 m square column located 0.9 m from one end of the tank. A volume of water (0.61 m wide, 0.4 m long and 0.3 m high) is initially contained behind a gate before being released. During the experiment a thin layer of water (10 mm deep) was also present in the tank downstream of the gate. A schematic of the set-up is shown in Figure 1.

For the present study, a total of eleven simulations were performed to investigate the influence that particle resolution, boundary conditions, fluid sound speed, viscosity and gate opening times has on the loading imparted to the column. Details of the main simulation parameters are summarised in Table 1. In all cases the fluid reference density was ρ_o = 1000 kg/m^3.

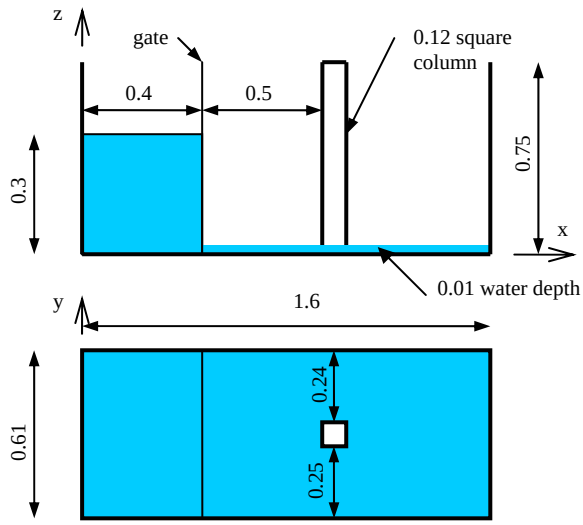

Figure 1: Schematic diagram of the geometry.

Case	Δp (mm)	Gate Opening (s)	Boundary Type	μ (kgm/s)	n
A	12	0	Repulsive	0.001	59223
B	12	0.1	Repulsive	0.001	59223
C	10	0	Repulsive	0.001	106051
F	5	0	Repulsive	0.001	744391
H	5	0	Press./cont.	0.001	891916
I	5	0	Repulsive	0.01	744391
J	5	0.05	Repulsive	0.001	744391
K	5	0.1	Repulsive	0.001	744391

Table 1: Summary of the simulation parameters.

In all simulations the column is modelled as an infinitely stiff rigid structure. That is to say, as the water impacts the column, the force is transmitted instantaneously to the measurement location. Typical simulation times on a single 3.2 GHz Xeon processor are 3 hrs, 30 hrs and 200 hrs for the 12mm, 10mm and 5mm simulations respectively.

RESULTS

A sequence of rendered images showing the flow of the water is shown in Figure 2.

A typical SPH time history of the net force acting on the column is shown in Figure 3. The force acting on the column was calculated by summing up the local forces (normal force/pressure and viscous) acting on the individual column particles. For comparison purposes the SPH results are filtered using a triangular-weighted double-sided moving time average (13 ms, ~100 pts) for the remainder of the paper, unless stated otherwise. Filtering is required since the real column is not perfectly rigid, the load cell measuring the impact load will have a finite response time and because the experimental data is sampled much less frequently.

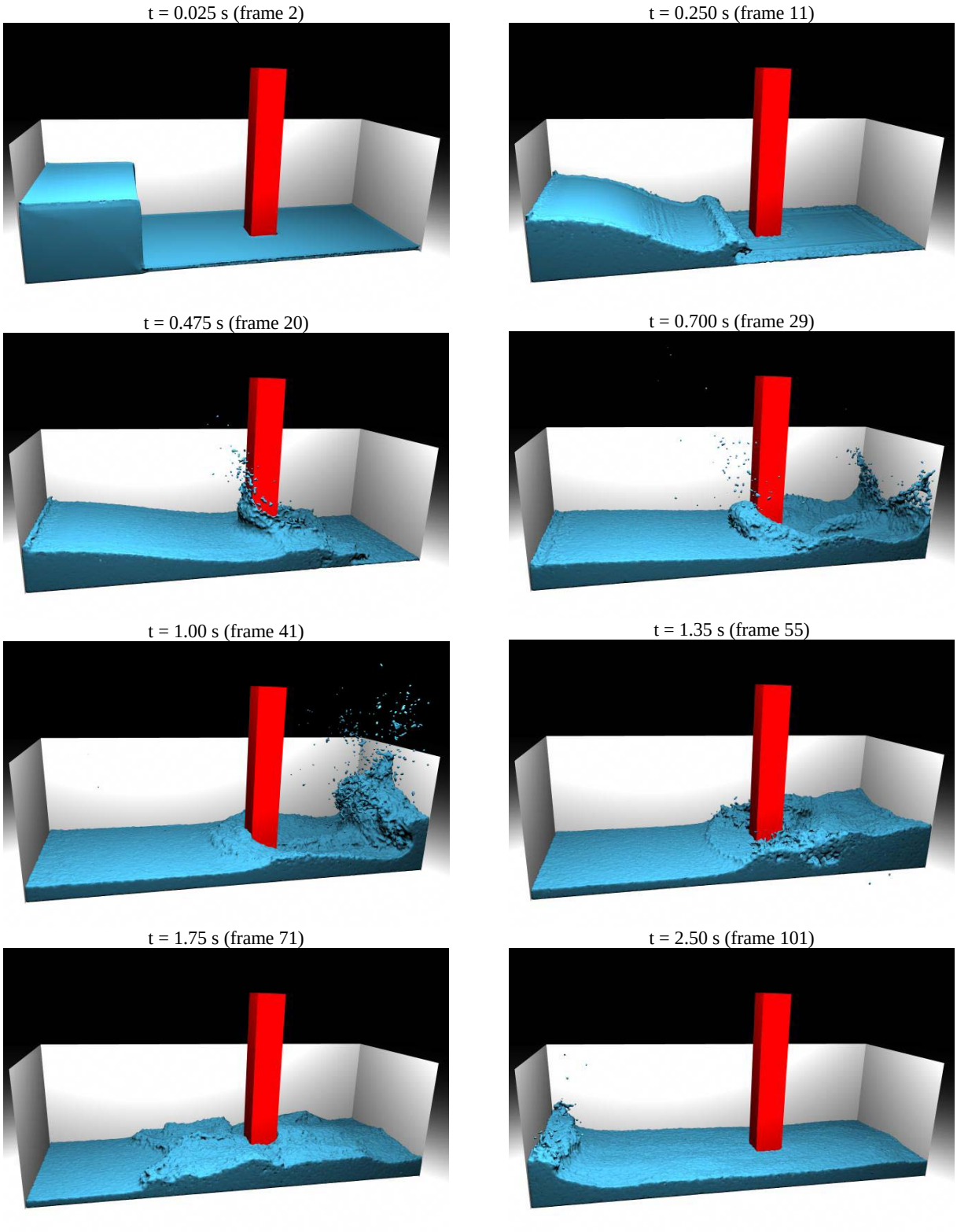

Figure 2: Sequence of images showing the evolution of the flow at various times (Case F).

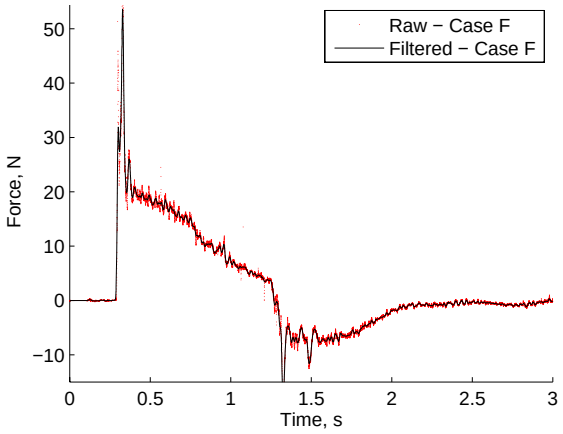

Figure 3: Raw and filtered SPH x-component net force acting on the column.

The primary features of the wave-structure interaction can be explained as follows with reference to Figure 2 and Figure 3. As the fluid is released (0 s) the volume of water collapses under the influence of gravity and the flow resembles a breaking bore (0.25 s). In practice, the breaking wave will entrain air, which can affect both the spatial and temporal loading characteristics (Greco et al. 2004) however in the simulations the gaseous phase is not modelled. As the fluid impacts the column (~0.33 s) it experiences a rapid increase in the net force (see Figure 3) followed by a sharp decline to around 40% of the peak force level. There follows a slow steady decrease in the net force as the fluid flows around either side of the column. Upon reaching the opposing wall (x = 1.6 m, ~0.7 s) the fluid is reflected and its bulk motion is in the negative x-direction. This causes a secondary impact on the rear face of the column causing a negative net force at t = 1.2 s. Following this, there is some residual wave motion which damps and the fluid approaches a static equilibrium and the net-force acting on the column approaches zero.

Comparison of Simulation and Experimental Column Forces

The simulated and measured net force acting on the column is shown in Figure 4. These results show that:

(a) the main features of the experimental[1] force measurements are in general reproduced well in the simulation.

(b) the computed peak force (see also Figure 9) is higher than the measured peak. Possible causes for this include: firstly, the column is modelled as infinitely stiff in the SPH simulations whereas there is a response time associated with the experimental measurements due to the finite stiffness of the column and response time of the load cell. Subsequently, sharp peaks will be spread out over some time. Secondly, the sample rate for experiments is much lower than the computations.

(c) it is also worth noting that the experimental data is comprised of more than one test which is particularly noticeable as the return wave impact the column at 1.3 s. Subsequently, the differences following this secondary impact are a real and unexplained difference.

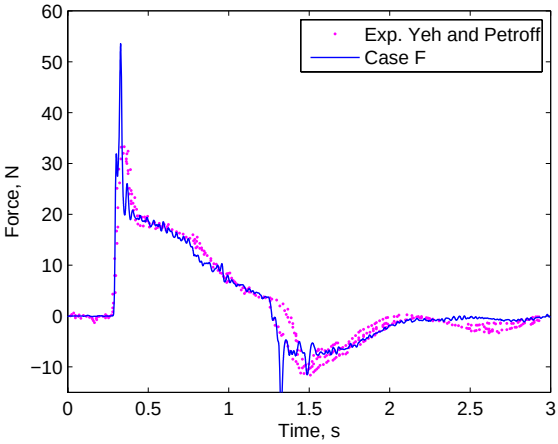

Figure 4: Experimental and simulated column net x-force time history.

Another important characteristic of a dynamic loading event is the impulse, which represents a change in momentum of the column. For a time varying force, the impulse (or cumulative impulse) is calculated discretely by,

$$I = \sum_{k} |\mathbf{F}|(t)\delta t$$

where $|\mathbf{F}|$ is the unfiltered net force acting on the column (boundary particles). To assist in the interpretation of the results, plots of the cumulative impulse are included in the remainder of the paper.

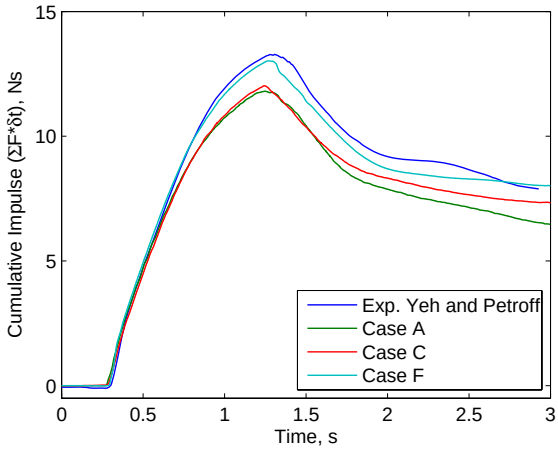

Figure 5: Cumulative impulse of the net force acting on the column for different particle resolutions.

Particle Resolution

Simulations using three different particle resolutions were performed to assess the influence of particle resolution on the column net force. Figure 5 shows the evolution of the impulse for the experimental data and computations using three different particle resolutions. It is evident from the figure that the SPH results approach the experimental values for increasing particle resolution. The finest resolution results (Case F) are shown to be in very good agreement for the primary impact period (0 s to ~1.2 s) however under-estimates the impulse following the secondary impact. To understand this further, additional

[1] The experimental time coordinate has been shifted to coincide with the SPH case F results.

simulations were performed using different boundary treatments, viscosities and finite gate opening times to assess their influence on the loading characteristics.

Viscosity

Simulations using two different values for the dynamic viscosity of the fluid were performed. Case F uses the actual dynamic viscosity of water while Case I uses a value an order of magnitude greater. It may be argued that in the absence of a suitable turbulence model, it may be more appropriate to use a higher-than-actual value when simulating relatively violent (turbulent) flows. Figure 6 shows the experimental data and SPH impulse time histories for two different dynamic viscosity values. The results indicate that the net force acting on the column is highly insensitive to the value of dynamic viscosity.

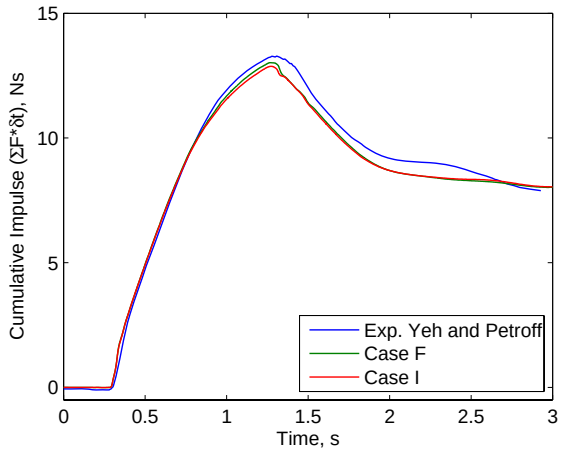

Figure 6: Cumulative impulse of the net force acting on the column for different fluid viscosities.

Boundary Treatment

Figure 7 shows the net force time history acting on the column for the two boundary treatments used along with the experimental data. The main differences between the two SPH results are that Case H predicts lower peak impact forces (primary and secondary) than Case F and for Case H there is a slight improvement following the secondary impact and residual wave motions.

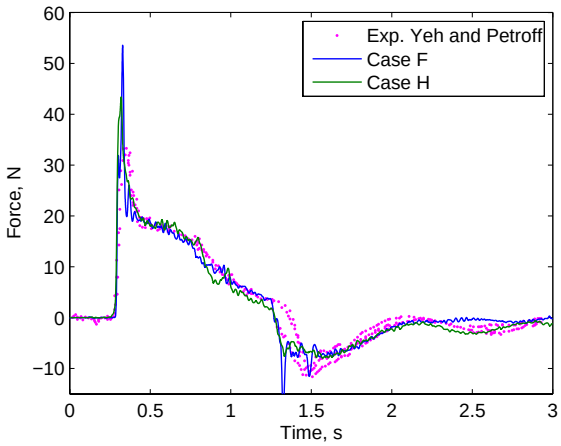

Figure 7: Column force for different boundary treatments.

Figure 8 shows the impulse time history for these two cases. Whilst Case H diverges slightly from the experimental curve following the initial impact it tends to match the experimental data better once the secondary wave starts to interact with the column. From these results the boundary implementation (press./cont.) based on the pressure calculation appear to be slightly better than the "repulsive" boundary, but both SPH results are very close to the experiment.

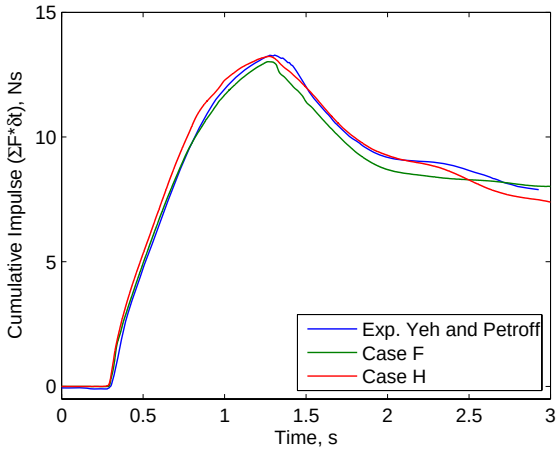

Figure 8: Cumulative impulse of the net force acting on the column for different boundary treatments.

Gate Opening Time

In the previous simulations, it has been assumed that the gate opened infinitely fast. The speed and manner of the gate removal can potentially influence the subsequent fluid motion so a gate removal model was included in the simulations. Three separate opening times for the gate were considered. In the first instance (Case F) the gate was assumed to open infinitely fast whereas Cases J and K utilised a finite opening time of 50 ms and 100 ms respectively. For cases J and K the gate was modelled as a row of boundary particles that were raised vertically at a constant velocity. The corresponding peak forces[2] acting on the column are shown in Figure 9.

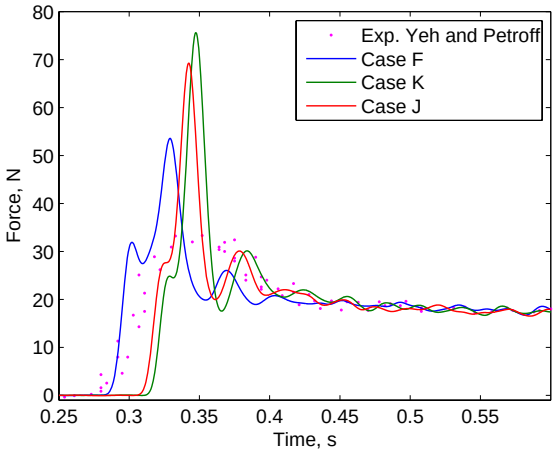

Figure 9: Column peak forces for various gate opening times.

[2] The gate commences opening at $t = 0$ s for all SPH simulations.

The main differences between the SPH results are that:

(a) the origin of the initial impact is delayed for slower opening times.

(b) the slower opening times produce higher peak impact forces. For these finite opening times, the flow retains a greater portion of its gravitational potential energy during the opening process. Prior to the impact, the rate in which the potential energy is transferred to kinetic energy is increased resulting in slightly higher peak loads than case F. Additional simulations are currently being performed to investigate this further.

(c) the finite opening time allows a higher net force magnitude to be maintained for longer (~1.3 s to 1.5 s) during the secondary impact.

In all cases the peak SPH results are considerably higher than the experiments. Once again, it is possible this may be due to the differences between the loading characteristics of the experimental apparatus and the computational model. Furthermore, it is not know whether the smaller peaks preceding and following the main peak values (see Figure 9) occur in practice or are unique to the single-phase SPH simulations. In the absence of additional data this cannot be confirmed. The impulse history for the various gate opening times are shown in Figure 10. The impulse for the finite opening time cases is shown to be marginally reduced as the opening time is increased. The results for the infinitely quick gate opening are in slightly better agreement with the experimental data. Overall, the results show that the main flow features are fairly insensitive to the speed of the gate lifting though there are noticeable differences in the primary wave arrival times and peak loads.

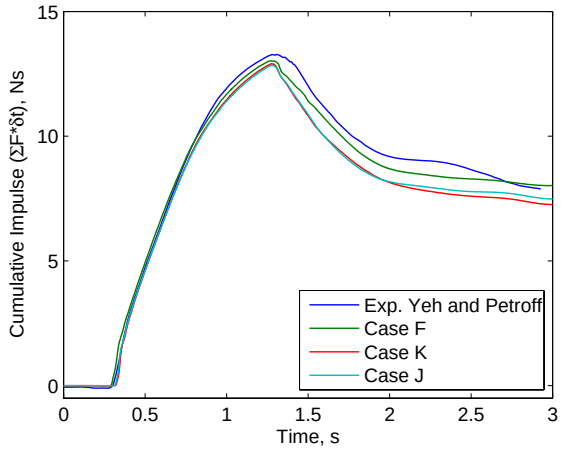

Figure 10: Cumulative impulse of the net force acting on the column for various gate opening times.

CONCLUSION

Three-dimensional Navier-Stokes SPH computations of a dam-break flow with a rectangular column located downstream have been performed. The simulations demonstrated the ability of SPH to quite accurately reproduce the transient loading characteristics on the column. The results were in excellent agreement with existing experimental data for the finest resolution simulation.

In all cases, SPH predicted higher peak impact loads than measured during the experiments. It was suggested that this may be attributed to (in part) the infinitely stiff assumption used in the structure model whereas in the experiments the column is not instantaneously responsive (i.e. it has finite stiffness) and there is also a response time associated with the load cell. Furthermore, air entrainment, which can affect the spatial and temporal loading characteristics, was not considered in the simulations.

Additional simulations were performed to assess the effect of various simulation parameters and options on the loading characteristics. The column loading was shown to be:

- insensitive to the fluid viscosity.
- slightly sensitive to the boundary treatment. Modelling the boundaries by including them in the pressure/continuity equation solution was shown to produce results in slightly better agreement with the experimental data, compared to those based on a normal repulsive force assumption.
- slightly sensitive to the speed of water release as controlled by the gate opening time. Slower opening times appear to slightly increase the peak load but reduce the impulse imparted to the column.

Further enhancements to the SPH method are being implemented to investigate the affect of air entrainment, turbulence and structure elasticity on wave-structure interactions.

AKNOWLEDGEMENTS

The authors would like to thank Joe Monaghan and Joseph Ha for providing assistance in understanding many of the fundamental aspects of SPH. The authors would also like to thank Geoff Robinson for his assistance in the data analysis.

REFERENCES

BUCHNER, B., (2002), "Green water on ship-type offshore structures", *Ph.D thesis.* Delft University of Technology, The Netherlands.

CLEARY, P.W., (1998), "Modelling confined multi-material heat and mass flows using SPH", *Applied Mathematical Modelling* **22**: 981-993.

CLEARY, P.W., PRAKASH, M., HA, J., STOKES, N. and SCOTT, C., (2005), "Smooth particle hydrodynamics: status and future potential", *Presented at 4th International Conference on CFD in the Oil and Gas, Metallurgical & Process Industries SINTEF / NTNU,* Trondheim, Norway.

ERSDAL, G. and KVITRUD, A., (2000), "Green water on Norwegian production ships", *Presented at Proceedings of the 10th International Offshore and Polar Engineering Conference*, Seattle, USA, May 28th - June 2nd.

FALTINSEN, O.M., LANDRINI M. and GRECO, M., (2004), "Slamming in marine applications", *Journal of Engineering Mathematics* **48**: 187-217.

GINGOLD, R.A. and MONAGHAN J.J., (1977), "Smoothed particle hydrodynamics: theory and application to non-spherical stars", *Monthly Notices of the Royal Astronomical Society* **181**: 375-389.

GÓMEZ-GESTEIRA, M. and DALRYMPLE, R.A., (2004), "Using a three-dimensional smoothed particle hydrodynamics method for wave impact on a tall structure", *Journal of Waterway, Port, Coastal and Ocean Engineering* **130**: 63-69.

GÓMEZ-GESTEIRA, M., (2006), "SPHERIC SPH benchmark test cases: Test 1 - Force exerted by a schematic 3D dam break on a square cylinder", http://cfd.me.umist.ac.uk/sph/TestCases/SPH_Test1.html.

GRECO, M., LANDRINI, M. and FALTINSEN, O.M., (2004), "Impact flows and loads on ship-deck structures", *Journal of Fluids and Structures* **19**: 251-275.

KLEEFSMAN, K.M.T., FEKKEN, G., VELDMAN, A.E.P., IWANOWSKI, B. and BUCHNER, B., (2005), "A Volume-of-Fluid based simulation method for wave impact problems", *Journal of Computational Physics* **206**: 363-393.

LUCY, L.B., (1977), "A numerical approach to the testing of the fission hypothesis", *Astronomical Journal* **82**: 1013-1024.

MONAGHAN, J.J., (1992), "Smoothed particle hydrodynamics", *Annual Review of Astronomy and Astrophysics* **30**: 543-574.

MONAGHAN, J.J., (1994), "Simulating free surface flows with SPH", *Journal of Computational Physics* **110**: 399-406.

MONAGHAN, J.J., (1995), "Simulating gravity currents with SPH: III Boundary Forces", *Rep. 95/11*, Department of Mathematics, Monash University, Melbourne, Australia.

MONAGHAN, J.J., (2005), "Smoothed particle hydrodynamics", *Reports on Progress in Physics* **68**: 1703-1759.

MONAGHAN, J.J. and LATTANZIO, J.C., (1985), "A refined particle method for astrophysical problems", *Astronomy and Astrophysics* **149**: 135-143.

RAAD, P.E. and BIDOAE, R., (2005), "The three-dimensional Eulerian-Lagrangian marker and micro cell method for the simulation of free surface flows", *Journal of Computational Physics* **203**: 668-699.

SPHERIC, (2006), "SPHERIC-SPH European Research Interest Community", http://cfd.me.umist.ac.uk/sph/.